Fuel Processing Technology 234 (2022) 107313

Contents lists available at ScienceDirect

Fuel Processing Technology

journal homepage: www.elsevier.com/locate/fuproc

Evaluation of oxygen carriers based on manganese-iron mixed oxides prepared from natural ores or industrial waste products for chemical looping processes

Beatriz Zornoza [a,b,*], Teresa Mendiara [a], Alberto Abad [a,*]

[a] Instituto de Carboquímica (ICB-CSIC), Miguel Luesma Castán 4, Zaragoza 50018, Spain
[b] Chemical and Environmental Engineering Department, Instituto de Nanociencia y Materiales de Aragón (INMA), Universidad de Zaragoza-CSIC, 50018 Zaragoza, Spain

ARTICLE INFO

Keywords:
Oxygen carrier
Low-cost materials
Manganese
Iron
Spinel
Magnetism

ABSTRACT

Manganese-iron mixed oxides have been identified as promising oxygen carrier materials in chemical looping processes. In this work, low-cost raw materials are considered for the production of this type of oxygen carrier. Four manganese based minerals from deposits of different locations – South Africa, Gabon(x2) and Brazil – and two iron based materials (Fe-ore from Spain and Redmud waste) were used to prepare suitable oxygen carriers through a new two-step production method: a mixing-grinding (about 5 μm) pre-treatment followed by pelletizing, crushing and sieving to produce particles of the desired size (100–300 μm). This method was required in order to form the MnFe mixed oxide and to provide permanent magnetic properties, which were not found when the oxygen carriers were prepared by the classical one-step method, i.e. crushing and sieving of raw materials to the desired particle size (100–300 μm). The oxygen uncoupling capability of the developed materials was extremely low and even completely lost after repeated redox cycles. However, they were reactive under chemical looping conditions with H_2, CO and CH_4. Reactivity varied with the raw materials used and with the redox cycles, being of crucial importance for its evolution the intensity of the chemical stress during hundreds of redox cycles.

1. Introduction

Chemical looping technologies are emergent processes allowing the conversion of carbonaceous fuels with inherent CO_2 capture [1]. The core of these processes is an oxygen carrier which transfer the oxygen required for the fuel conversion from the air to the fuel. In this way, direct contact of the air with the fuel is avoided and, therefore, the resulting gases from the fuel conversion are not diluted in N_2 from air. Often, an oxygen carrier is based on a metal oxide, which is cyclically used: oxygen in metal oxide is used for the fuel conversion and then, the depleted oxygen carrier is regenerated by air. In a preferred configuration, the oxygen carrier is continuously circulating between two fluidized bed reactors [2]: the fuel reactor where the fuel is converted; and the air reactor where the oxygen carrier is oxidized by air [3]. Therefore, the oxygen carrier is prepared in the form of fluidizable particles [4]. General requirements for an oxygen carrier are the followings: suitable thermodynamic properties for the fuel conversion, high reactivity and oxygen transport capacity, high mechanical strength to be attrition resistant, low agglomeration tendency, mechanical and chemical stability in successive redox cycles, environmental friendly and low cost [5].

Fig. 1 shows a classical classification of the chemical looping processes [6], which allows to use these technologies for heat, power and/or hydrogen poly-generation [7]. In chemical looping combustion (CLC), the objective is to produce energy (heat, electricity) by the complete combustion of the fuel to CO_2 and H_2O. Ni, Cu, Mn and Fe oxides have been extensively evaluated as active compounds for CLC considering the following reactions for the oxygen transference for a fuel with a general composition $C_xH_{2y}O_z$:

$$(2a+b-c)\ NiO + C_aH_{2b}O_c \rightarrow (2a+b-c)\ Ni + a\ CO_2 + b\ H_2O \quad (R1)$$

$$(2a+b-c)\ CuO + C_aH_{2b}O_c \rightarrow (2a+b-c\ Cu + a\ CO_2 + b\ H_2O \quad (R2)$$

$$(2a+b-c)\ Mn_3O_4 + C_aH_{2b}O_c \rightarrow 3(2a+b-c)\ MnO + a\ CO_2 + b\ H_2O \quad (R3)$$

* Corresponding authors.
E-mail addresses: bzornoza@unizar.es (B. Zornoza), abad@icb.csic.es (A. Abad).

https://doi.org/10.1016/j.fuproc.2022.107313
Received 22 February 2022; Received in revised form 25 April 2022; Accepted 4 May 2022
Available online 25 May 2022

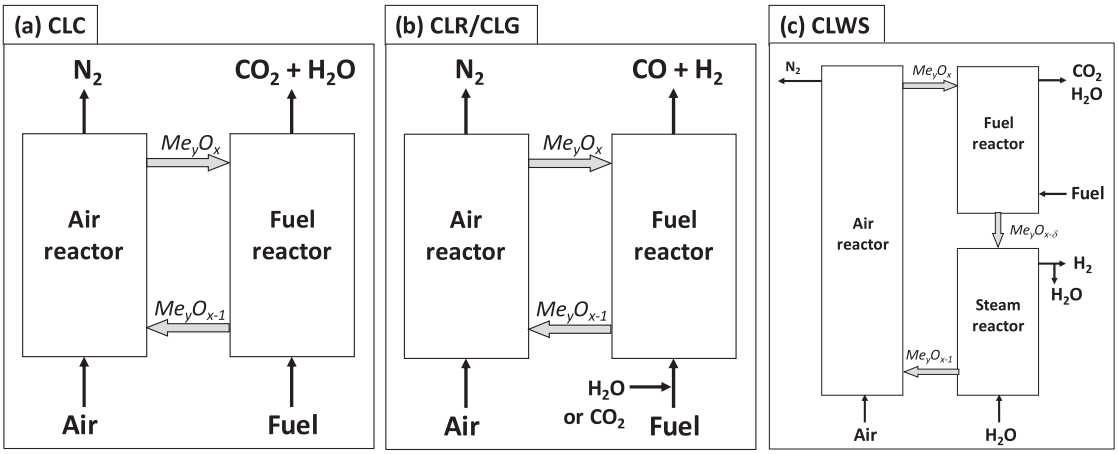

Fig. 1. Scheme of the chemical looping combustion(CLC), chemical looping reforming (CLR) or gasification (CLG) and chemical looping with water splitting (CLWS) processes.

$$3(2a+b-c)\ Fe_2O_3 + C_aH_{2b}O_c \rightarrow 2(2a+b-c)\ Fe_3O_4 + a\ CO_2 + b\ H_2O \quad (R4)$$

In Chemical looping reforming (CLR) or gasification (CLG), a partial oxidation of the fuel to syngas is performed by limiting the amount of oxygen transferred. The CO/H_2 ratio may be modified by adjusting the steam/fuel ratio or performing the dry-methane reforming or dry-gasification with CO_2 as reforming/gasifying agent.

The purpose of Chemical looping with Water Splitting (CLWS) – also known as chemical looping hydrogen generation (CLHG) or three reactors chemical looping (TRCL) – is the production of a separated H_2 stream in the steam reactor [8]. The CLWS system consists of three reactors: fuel, air and steam reactors. Often Fe-based materials are developed for this process as FeO or Fe may be oxidized by steam to produce H_2 in the steam reactor:

$$3\ Fe + 4\ H_2O \rightarrow Fe_3O_4 + 4\ H_2 \quad (R5)$$

$$3\ FeO + H_2O \rightarrow Fe_3O_4 + H_2 \quad (R6)$$

Therefore, the Fe_2O_3 reduction degree in the CLWS fuel reactor must be higher than in CLC.

$$(2a+b-c)\ Fe_2O_3 + C_aH_{2b}O_c \rightarrow 2(2a+b-c)\ FeO + a\ CO_2 + b\ H_2O \quad (R7)$$

$$(2a+b-c)/3\ Fe_2O_3 + C_aH_{2b}O_c \rightarrow 2(2a+b-c)/3\ Fe + a\ CO_2 + b\ H_2O \quad (R8)$$

NiO has some thermodynamic limitation to achieve complete conversion of the fuel to CO_2 and H_2O, with minor amounts of H_2 and CO at equilibrium conditions. Anyway, the fuel selectivity to CO_2 and H_2O is as high as 98–99%, and this would not be an impediment to its use in CLC. This material is highly suitable for the CLR process due to the catalytic activity of metallic Ni on the methane reforming. However, Ni is an expensive metal with serious environmental concerns, which makes mandatory the development of highly durable particles to be used for long term periods.

Cu-based oxygen carriers are highly reactive materials allowing the complete combustion in CLC, but the operating temperature is usually limited below 900–950°C due to the low melting point of copper [9]. Also, Cu-based materials may be used in CLR to produce syngas with high methane conversion [10]. In addition, CuO has the interesting capability of releasing molecular O_2 following reaction (R9), which is of special interest for its use with solid fuels in the so-called chemical looping with oxygen uncoupling process (CLOU) [11].

$$2\ CuO \rightarrow Cu_2O + 0.5\ O_2 \quad (R9)$$

In general, Mn- and Fe-based oxygen carriers are less reactive than materials based on Ni or Cu. Therefore, manganese and iron oxides are not recommended for the combustion of gaseous fuels, unless preparation method was optimized to develop oxygen carriers with high enough reactivity to be used with gaseous fuels such as natural gas [5]. However, these oxides have been extensively used for combustion of solid fuels [12,13]. Main reasons are that reactivity of the oxygen carrier material is not a decisive factor to achieve high conversion rates of the solid fuel, as they are limited by the slow gasification rate and the poor gas-solid contact between volatile matter, which may be emitted in plumes inside the fluidized bed reactor, and the solid oxygen carrier. In addition, due to the presence of ash in the solid fuels, a loss of oxygen carrier particles is expected in the ash drain stream [14], in addition to the existence of the non-desired interaction of the active metal oxide with ash components such as K, Na or P [15]. These facts may cause a high renewal of the material in the system. In this sense, the great advantage of Mn and Fe is that they are cheap and environmental friendly, being also beneficial for the ash disposal.

Thermodynamic restrictions limit the reduction of Fe_2O_3 to Fe_3O_4 to allow the complete combustion of fuel to CO_2 and H_2O in CLC. Further reduction to FeO or Fe causes the presence of a relevant fraction of H_2 and CO in the combustion gases. However, the oxygen use in Fe_2O_3 for CLC may be extended by forming mixed oxides; e.g. reaction (R10), allowing the complete oxidation of the fuel to CO_2 and H_2O with ilmenite. In addition, the capability of iron oxide to be reduced to FeO or Fe may be exploited in the CLWS process; see reactions (R5)–(R8).

$$(2a+b-c)\ Fe_2TiO_5 + (2a+b-c)\ TiO_2 + C_aH_{2b}O_c \rightarrow 2(2a+b-c)\ FeTiO_3 + a\ CO_2 + b\ H_2O \quad (R10)$$

Regarding to Mn, its oxygen uncoupling capability is limited by the difficulty to be oxidized to Mn_2O_3 [16], being restricted the oxidation by air to Mn_3O_4 in most of cases. The complete oxidation to Mn^{3+} is favoured by forming mixed oxides, e.g. with Fe, Ca, Mg or Si [17].

Among oxygen carriers prepared from low cost metals for CLC, MnFe mixed oxides stand out due to its relatively high reactivity and oxygen transport capacity, their oxygen uncoupling capability and their magnetic properties [18,19]. The oxygen uncoupling capability in MnFe mixed oxide can be exploited by reacting between bixbyite and spinel phases – reaction (R11). Also, MnFe-spinel is able to burn a fuel using lattice oxygen, being reduced to mangano-wüstite – reaction (R12).

$$3\ (Mn_xFe_{1-x})_2O_3 \rightarrow 2\ (Mn_xFe_{1-x})_3O_4 + 0.5\ O_2 \quad (R11)$$

$$(2a+b-c)\ (Mn_xFe_{1-x})_3O_4 + C_xH_{2y}O_z \rightarrow 3(2a+b-c)\ Mn_xFe_{1-x}O + a\ CO_2 + b\ H_2O \quad (R12)$$

The presence of iron in the MnFe mixed oxides makes these materials

Table 1
Mn and Fe content of the minerals/waste, as received, by ICP.

Sample	Description/Origin	% Mn	% Fe	Other major compounds
MnSA	Mn-ore from South-Africa Supplied by FerroAtlántica del Cinca[4]	42.1 ± 5.6	12.7 ± 3.0	Si [1]
MnGBHNE	Mn-ore from Gabon Supplied by FerroAtlántica del Cinca[4]	42.0 ± 5.0	4.6 ± 0.5	Si, Al [1]
MnGBMPB	Mn-ore from Gabon Supplied by Mario Pilato Blatt	50.7 ± 2.3	2.5 ± 1.1	Si, Al [1]
MnBR	Mn-ore from Brasil Supplied by Mineração Buritirama	44.7 ± 1.0	3.0 ± 1.3	Si, Al [1]
Fe-ESF	Industrial waste, Fe-enriched sand fraction Supplied by Alcoa	0.06 ± 0.03	42.1 ± 1.5	Al, Na, Ti [2]
Fe-ore Tierga	Europe-Alúmina Española Fe-ore from Spain Supplied by Promindsa	0.06 ± 0.03	52 ± 1.6	Si, Ca, Al, Mg [3]

[1] Minor amounts (0.1–1%) of Ca, K, Mg, Na, and Ti [32]
[2] Minor amounts (0.1–1%) of Ca, Cr, K, Mg, Si, and V [14]
[3] Minor amounts (0.1–1%) of Cr, K, and Ti [14]
[4] Former Hidro Nitro Española S.A.

also suitable for CLWS from a thermochemical point of view [20]. The mixed oxide may be highly reduced to MnO + Fe – reaction (R13)–, and then oxidized to mangano-wüstite by steam – reaction (R14). Also, a fraction of mangano-wüstite may be oxidized to spinel by steam – reaction (R15).

$$(2a+b-c)/(1-x)\ Mn_xFe_{1-x}O + C_aH_{2b}O_c \rightarrow x(2a+b-c)/(1-x)\ MnO + (2a+b-c)\ Fe + a\ CO_2 + b\ H_2O \quad (R13)$$

$$x\ MnO + (1-x)\ Fe + (1-x)\ H_2O \rightarrow Mn_xFe_{1-x}O + (1-x)\ H_2 \quad (R14)$$

$$3\ Mn_xFe_{1-x}O + H_2O \rightarrow (Mn_xFe_{1-x})_3O_4 + H_2 \quad (R15)$$

For the use of MnFe mixed oxides in CLWS, the required deep reduction might compromise the chemical and mechanical stability of the oxygen carrier. For example, it may provoke the weakening of the solid structure by phenomena as cracks building up. Also, ionic migration of the metals provokes metal segregation, affecting to the chemical stability. In addition, agglomeration is also promoted by a deep reduction, which may affect to the reactivity or fluidization capability. All these aspects need to be evaluated.

In addition, the $(Mn_xFe_{1-x})_3O_4$ spinel shows magnetic properties which may be of interest for the separation of oxygen carrier particles from ash with solid fuels, allowing the re-use of oxygen carrier particles and minimizing the make-up flow of new oxygen carrier [21].

MnFe mixed oxides prepared from highly pure metal oxides at lab-scale have shown good performance for the combustion of gaseous [22] and solid fuels [23], with improved results compared to mono-metallic Mn or Fe oxides [19,24]. For the scale-up of these materials to ton-scale, the use of low cost raw materials – such as natural ores or industrial wastes – would be preferred instead of chemical grade metal oxides.

Some oxygen carriers have been synthetized from low-cost raw material with the objective of being prepared on a ton-scale. For example, $CaMnO_3$-based perovskites doped with Mg and Ti were first prepared from high purity raw materials to evaluate its performance as oxygen carrier and to be tested at lab-scale [25]. Then, this material was replicated at ton-scale by using $Ca(OH)_2$, Mn-based ores or industrial wastes and anatase as low cost raw materials for Ca, Mn and Ti sources, respectively [26]. Copper ferrites have been also considered to be used as oxygen carriers [27]. Considering the high cost of copper, oxygen carriers based on copper and iron has been synthetized using copper ore and hematite as raw materials [28]. Fine particles of raw materials (<100 μm) were mechanically mixed to produce oxygen carrier particles in the desired size of 100–300 μm either by wet mixing, extrusion-spheronization [29] or spray drying [30]. Alternatively, redmud may be used also as the iron source [31].

In a previous work, a Mn-ore with high iron content was selected for the preparation of oxygen carrier particles [32]. Following the usual procedure for natural ores, oxygen carrier particles were prepared in the suitable particle size (100–300 μm) by crushing and sieving; then, particles were calcined at high temperature. The calcined material did not show the formation of the desired MnFe mixed oxide, but it was composed by a mixture of Mn_3O_4 and Fe_2O_3. However, the presence of MnFe mixed oxide was confirmed in oxygen carrier particles with similar Mn:Fe ratio but synthetized from fine chemical powders of Mn and Fe oxides, which were in the size of a few microns [33]. Therefore, it is believed that the low particle size of raw materials improved the Mn-Fe contact, and therefore the formation of MnFe mixed oxide was promoted.

The objective of this work is the production and characterization of oxygen carriers based on MnFe mixed oxides using low-cost raw materials as manganese and iron sources, such as Mn- and Fe-ores, or an industrial waste from the aluminium production – Fe-enriched sand fraction (Fe-ESF) or redmud. The production method was adapted in order to promote the formation of the MnFe mixed oxide in the oxygen carrier particles. The adequacy of the prepared materials to be used in CLC is evaluated considering the reactivity, oxygen transport capacity, crushing strength, magnetic properties and stability during hundreds of redox cycles under characteristic conditions of low and high chemical stress. In addition, a preliminary evaluation of the suitability of these materials for CLWS was done by performing the required deep reduction in the redox cycles.

2. Experimental section

2.1. Materials

We focus our study in the preparation of oxygen carriers in the proportion Mn/Fe of 0.77/0.23. Minerals previously evaluated as oxygen carriers based on Mn – MnSA, MnGBHNE, MnGBMPB and MnBR [32] – and Fe – Fe-ore Tierga [34]–, as well as one Fe-based industrial waste – Fe-ESF or redmud – [35] were selected as raw Mn and Fe sources. Table 1 shows the ICP analysis of the original Mn and Fe materials. Based on these results, the corresponding mixtures of every Mn ore with each Fe material were prepared; see Supplementary Material (SM) for details. Note that MnSA mineral has the target Mn/Fe ratio because its relatively high Fe content. In this case, it was not required the addition of another material as a Fe source. Considering the three remaining Mn minerals, they were mixed with the corresponding amount of either Fe-ore or redmud to achieve the desired Mn/Fe molar ratio. Therefore, seven different oxygen carriers were prepared in total; see Table S1 in SM.

The objective of this work was to produce the MnFe mixed oxide by mixing and calcining the Mn and Fe materials. Raw materials were in the form of coarse particles (from 0.1 to 10 mm) as received. However, the formation of the MnFe mixed oxide is not promoted by calcining these coarse particles [32]. In order to promote the formation of the desired MnFe mixed oxide, we explore in this work the calcination of a mixture of finer particles. For that, a grinding pre-treatment of the prepared solid mixture with the target Mn/Fe ratio was done achieving particle sizes of about 5–10 μm and, at the same time, improving the Mn-Fe contact by mechanical activation. Details about the grinding method are found in SM (see also Table S1).

After milling, subsequent pelletizing was performed. Cylindrical pellets (ca. 10 mm diameter, 20 mm height) were prepared by cold compression at 16 MPa for 60 s using a hydraulic press (HJE 5-5model).

Table 2
Physic-chemical characterization of oxygen carrier particles: chemical composition, purity of MnFe mixed oxide, main crystalline phases by XRD analysis, magnetic permeability and crushing strength.

Sample	% metal[a]		$(Mn_xFe_{1-x})_yO_z$		% metal oxide		Purity[b]	XRD main crystalline phases[c]	Magnetic permeability (−)	Crushing strength (N)
	Mn	Fe	x	1-x	Mn_3O_4	Fe_3O_4				
MnSA	40.7	17.7	0.70	0.30	56.5	24.5	81.0	$(Mn_xFe_{1-x})_3O_4$, Mn_3O_4, $CaSiO_3$	1.9	3.0
MnGBHNE+Fe-ESF	41.4	14.5	0.74	0.26	57.5	20.0	77.5	$(Mn_xFe_{1-x})_3O_4$, $(Mn_xFe_{1-x})_2O_3$	1.2	3.8
MnGBHNE+Fe-ore	40.4	15.6	0.72	0.28	56.1	21.6	77.6	$(Mn_xFe_{1-x})_3O_4$, $(Mn_xFe_{1-x})_2O_3$	2.3	3.0
MnGBMPB+Fe-ESF	44.4	15.1	0.75	0.25	61.6	20.9	82.5	$(Mn_xFe_{1-x})_3O_4$, $FeMnO_3$, Mn_3O_4	1.4	2.0
MnGBMPB+Fe-ore	45.2	16.4	0.73	0.27	62.8	22.7	85.4	$(Mn_xFe_{1-x})_3O_4$, $FeMnO_3$, Mn_3O_4	1.7	3.1
MnBR+Fe-ESF	40.7	14.3	0.74	0.26	56.5	19.8	76.3	$(Mn_xFe_{1-x})_3O_4$, $FeMnO_3$, Mn_3O_4	1.3	2.4
MnBR+Fe-ore	40.6	15.6	0.72	0.28	56.4	21.6	77.9	$(Mn_xFe_{1-x})_3O_4$, $FeMnO_3$, Mn_3O_4	1.5	2.5
Mn77Fe[d]	52.9	16.8	0.77	0.23	76	24	100.0	$(Mn_xFe_{1-x})_2O_3$	1.0	2.7
Mn77Fe[SD]1350[d]	52.9	16.8	0.77	0.23	76	24	100.0	$(Mn_xFe_{1-x})_3O_4$, Mn_3O_4	2.5	1.7

[a] Note that the sum of other metals different to Mn and Fe (i.e. Al, Ca, K, Mg, Si and Ti) is ≤10%
[b] Purity by ICP, calculated as $\%Mn_3O_4 + \%Fe_3O_4$
$(Mn_xFe_{1-x})_3O_4$: Jacobsite/Spinel; Fe_3O_4: Magnetite; Mn_3O_4: Hausmannite; $CaSiO_3$: Wollastonite; $(Mn_xFe_{1-x})_2O_3$: Bixbyite
It was not possible to identify the exact composition in $(Mn_xFe_{1-x})_3O_4$ by XRD analysis due to low effect of stoichiometry on cell parameters
[c] XRD diffractograms of the 7 prepared materials are shown in Fig. S1 in SM
[d] Oxygen carriers from metal oxides of chemical grade as raw materials and prepared by pelletization and calcined at 950°C (Mn77Fe) [33] or prepared by spray drying and calcined at 1350°C (Mn77Fe[SD]1350) [21]

These pellets were further calcined at 950°C for 4 h to increase the mechanical strength of the particles. Then, they were crushed and sieved into the proper particle size to be used as oxygen carrier in chemical looping processes, namely 100–300 μm.

2.2. Physical and chemical characterization

Different techniques were applied to perform physical and chemical characterization on the different Mn-Fe oxygen carriers prepared in this work from low-cost raw materials. The identification of the crystalline chemical species was carried out by X-ray diffraction (XRD) in a Bruker D8 Advance X-ray powder diffractometer equipped with an X-ray source with a Cu anode working at 40 kV and 40 mA and an energy-dispersive one-dimensional detector. The diffraction pattern was obtained with a scanning rate of 0.02° over the 2θ range of 10–80°. The composition of the different materials was determined by inductively coupled plasma mass spectrometry (ICP-MS) using an ICP Jobin Ybon apparatus. Particle size distribution (PSD) of the materials was obtained in a Beckman Coulter LS13320 particle size analyzer by applying the laser diffraction technique (ISO13320 standard). The magnetic permeability was measured using a Bartington single frequency MS2G sensor connected to a magnetic susceptibility MS3 meter. Mechanical strength of the particles was determined using a Shimpo FGN-5× crushing strength apparatus. At least 20 measurements of particle fracture were taken to give the average value of the force. The microstructure of the oxygen carrier materials was explored trough a scanning electron microscope SEM EDX Hitachi S-3400 N equipped with an EDX analyzer Röntec XFlash of Si (Li). Both the morphology of the particles and their cross section were observed after fracturing once embedded in resin.

2.3. Thermogravimetric analyzer (TGA)

The oxygen transport capacity (R_{OC}) and the reactivity of the oxygen carrier materials were determined using a thermogravimetric apparatus (TGA), CI Electronics type operating at atmospheric pressure. For a general evaluation of the seven Mn-Fe oxygen carriers, approximately 50 mg of sample was loaded in a platinum basket suspended inside a quartz reactor.

The capability of the oxygen carrier materials to react with reducing gases was also evaluated. In this case, the material can be reduced up to mangano-wüstite (MW). For that, once the desired temperature (950°C) is reached three consecutive redox cycles were conducted alternating reduction with H_2, CO or CH_4 and oxidation in air. These conditions were selected in order to compare the reactivity of the MnFe oxygen carriers prepared in this work with those materials based on highly pure Mn and Fe oxides and those solids used as raw materials.

The oxygen transport capacity during redox cycles was determined in TGA by using 5% H_2 together with a high H_2O concentration (40%) in order to prevent the reduction of mangano-wüstite to a mixture of MnO and metallic Fe [20]. For steam addition, the reacting gas was saturated at the equilibrium vapor pressure by bubbling through a temperature-controlled saturator containing water. The oxygen transport capacity, R_{OC}, is defined in Eq. (1) as the mass fraction that can be used in the oxygen transfer.

$$R_{OC} = \frac{m_o - m_r}{m_o} \tag{1}$$

where m_o and m_r are the mass of oxidized and reduced sample, respectively.

The solid conversion for the reduction, X_r, and oxidation, X_o, of the Mn-Fe-oxygen carriers were calculated from the mass variations registered in TGA, according to Eq. (2) and Eq. (3), respectively:

$$X_r = \frac{m_o - m}{R_{oc} m_o} \tag{2}$$

$$X_o = \frac{m - m_r}{R_{oc} m_o} \tag{3}$$

where m is the instantaneous mass of the sample.

Reactivity to CO and CH_4 was determined in 15% CO + 20% CO_2, or 15% CH_4 + 20% H_2O mixtures, balanced by N_2 respectively. The concentration of 15% was used to facilitate the reactivity comparison between different materials following the methodology based on the calculation of the *Rate index* and proposed by Johansson et al. [36]. In the case that a different gas concentration was used, the reactivity was normalized to a concentration of 15% following the same methodology. To evaluate the reaction rate of the Mn-Fe-based oxygen carriers, the normalized rate index (RI) was calculated by applying Eq. (4):

$$Rate\ Index\ (\mathrm{RI}, \%/min) = 60 \cdot 100 \cdot \frac{P_{ref}}{P_{TGA}} \cdot \frac{1}{m_o} \left[\frac{dm}{dt}\right]_{X=0} \tag{4}$$

where P_{TGA} is the partial pressure of the reacting gas in TGA; P_{ref} is the reference partial pressure of the reacting gas: 0.15 atm for the reduction (H_2, CO_2, or CH_4) and 0.10 atm for the oxidation (O_2); m_0 is the initial mass of the sample; and m is the mass of oxygen carrier. The reaction rate (dm/dt) was calculated for zero conversion.

Additionally, to check the stability and durability of the selected oxygen carriers 300 reduction-oxidation cycles were performed under

Table 3
Theoretical and experimental oxygen transport capacity for the oxygen uncoupling reaction during N_2/air cycles performed at 870°C.

Sample	$R_{OC,CLOU}$ (%)				Theoretical $R_{OC,CLOU}$ (%)[1]	Conversion to bixbyite	
	N_2		O_2 (air)				
	Cycle 1	Cycle 3	Cycle 1	Cycle 3		Before Cycle 1	Cycle 3
MnSA	0.08	0.03	0.06	0.02	2.73	3.0	1.1
MnGBHNE+Fe-ESF	2.17	0.12	0.18	0.11	2.61	83.1	4.6
MnGBHNE+Fe-ore	2.17	0.04	0.35	0.03	2.62	83.0	1.5
MnGBMPB+Fe-ESF	1.73	0.05	0.53	0.05	2.78	62.2	1.8
MnGBMPB+Fe-ore	1.20	0.00	0.58	0.00	2.88	41.5	0.0
MnBR+Fe-ESF	1.58	0.10	0.38	0.09	2.57	61.6	3.9
MnBR+Fe-ore	1.32	0.02	0.12	0.02	2.63	50.3	0.8

[1] According to the Mn/Fe ratio and purity in Table 2

Table 4
Theoretical values of the oxygen transport capacity for pure MnFe mixed oxide and the actual theoretical oxygen transport capacity in the prepared oxygen carrier for the spinel reduction either to mangano-wüstite or to a MnO + Fe mixture.

Sample	Redox pair			
	Spinel-Mangano-wüstite		Spinel-(MnO + Fe)	
	$R^t_{OC,\ pure}$ (%)	R^t_{OC} (%)	$R^t_{OC,\ pure}$(%)	R^t_{OC}(%)
MnSA	7.0	5.6	13.2	10.7
MnGBHNE+Fe-ESF	7.0	5.4	12.3	9.6
MnGBHNE+Fe-ore	7.0	5.4	12.7	9.9
MnGBMPB+Fe-ESF	7.0	5.8	12.2	10.1
MnGBMPB+Fe-ore	7.0	6.0	12.5	10.7
MnBR+Fe-ESF	7.0	5.3	12.3	9.4
MnBR+Fe-ore	7.0	5.4	12.7	9.9

conditions at which either high or low variation of the oxygen carrier conversion was achieved. For that, the H_2 concentration and reacting time was fixed at: (1) 2% H_2 for 36 s for low conversion variation; and (2) 10% H_2 for 42 s for high conversion variation. The oxidation period was carried out with 10% of oxygen during 120 s to guarantee a high regeneration degree during the redox cycles. After that, one extra cycle using H_2, CH_4 or CO as reducing gases were done to determine the reactivity variation after 300 redox cycles and test the durability of the material.

To analyze the oxygen uncoupling properties due to the reaction from bixbyite to spinel phases, decomposition-regeneration cycles were performed alternating highly-pure N_2 (<2 ppm O_2) and air at temperature of 870°C. During the stage in N_2, reduction to spinel was guaranteed. In addition, oxygen concentration at 21 vol% was used during the oxidation period to evaluate the ability to regenerate bixbyite.

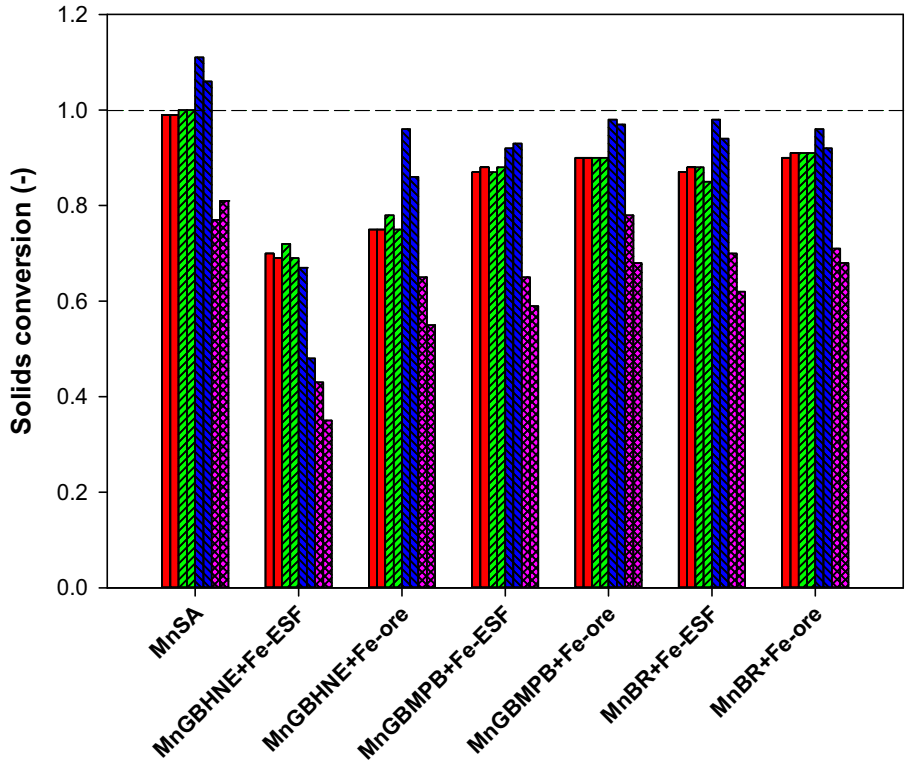

Fig. 2. Solids conversion reached for the 7 oxygen carriers in cycle 1 and cycle 3 during reduction with 5% H_2 + 40% H_2O (), subsequent oxidation in air after reduction in H_2 (), reduction with 15% CO + 20% CO_2 () or reduction with 15% CH_4 + 20% H_2O ().

Table 5
Actual oxygen transport capacity for the spinel-mangano-wüstite redox system in 5%H_2 + 40%H_2O, as well as the estimated values for a physical mixture of the raw materials.

Sample	*Actual R_{OC} for MnFe mixed oxide*	Estimated R_{OC} for Mn_3O_4 + Fe_2O_3 mixture
MnSA	5.6	4.8
MnGBHNE+Fe-ESF	3.8	4.7
MnGBHNE+Fe-ore	4.1	4.6
MnGBMPB+Fe-ESF	5.0	5.0
MnGBMPB+Fe-ore	5.4	5.1
MnBR+Fe-ESF	4.6	4.6
MnBR+Fe-ore	4.9	4.7

3. Results

3.1. Characterization of the prepared oxygen carriers

The 7 oxygen carrier materials were analyzed by ICP to determine the current Mn and Fe content in the prepared samples; see Table 2. However, although the oxygen carriers were prepared with the target of having a Mn/Fe molar ratio of 77/23, as the previously studied synthetic material, the molar Mn/Fe ratios obtained in the prepared particles were somewhat lower than the target value, with ratios between 70/30 and 75/25. This may be due to the inhomogeneity in the raw samples, as it is expected for natural ores or industrial waste products. This fact is corroborated by the deviation in the Mn and Fe content showed in Table 1. Another difference was the purity. Obviously, materials from chemical grade metal oxide were highly pure; but the purity of the oxygen carriers prepared from low cost materials are in the range of 76 to 85% due to raw materials were not pure metal oxides; see Tables 1 and 2.

XRD analysis shows that most of Mn and Fe was in a MnFe mixed oxide in the spinel phase; see Table 2. Some small amounts of bixbyite and hausmannite were also detected. Note that bixbyite formation was thermodynamically possible under the used calcining conditions, i.e. 950°C in air [20]. The formation of the MnFe mixed oxides validates the preparation method to obtain spinel or bixbyite phases. This finding was different to what happened when the materials were calcined after crushing to the suitable particle size of the oxygen carrier, namely 100–300 μm. For example, MnSA material has Mn and Fe at a suitable proportion to form the desired MnFe mixed oxide. However, independent Mn and Fe oxides were formed instead of the MnFe mixed oxide when MnSA was crushed and sieved to 100–300 μm and then calcined [32]. This fact was justified by a poor contact between Mn and Fe grains due to the relatively big particle size. In this work, the contact between Mn and Fe grains was improved by decreasing the particle size to 5–10 μm during the milling process; see the description of the preparation process in SM. As a result, the MnFe mixed oxide was formed after calcination. This result was similar to the preparation of the Mn77Fe mixed oxide from metal oxides of chemical grade [33].

However, the synthetic Mn77Fe material was mainly formed by the bixbyite phase, while the main phase in materials prepared from natural ores or industrial wastes was the spinel phase. A similar synthetic material prepared by spray drying was calcined at a higher temperature, namely 1350°C [21]. In this case, the main crystalline phase was the spinel due to its difficulty to be oxidized to bixbyite. Therefore, it can be concluded that the spinel formed in the MnFe mixed oxides prepared from low-cost Mn and Fe materials may show some inhibitory effect making the spinel oxidation so slow that it did not form during the calcination period. This fact will be later confirmed during the reactivity tests in TGA; see Sections 3.2 and 3.3.

The crystalline phases in the particles have a relevant effect on the magnetic permeability, which is in the range between 1.3 and 2.3 for the prepared oxygen carriers from low-cost materials. It was observed that these values are slightly higher when Fe-ore is added to the Mn mineral. This magnetic behavior is provided by the existence of the MnFe mixed oxide in the spinel phase. Thus, the synthetic material Mn77Fe, which is characterized by the complete oxidation to bixbyite, did not show magnetic behavior. On the contrary, the magnetic behavior was revealed when the oxidation of spinel to bixbyite was inhibited, e.g. by calcining the Mn77Fe material to a higher temperature, e.g. 1350°C in Mn77Fe[SD]1350; see Table 2.

Finally, attending to the crushing strength of particles, all combinations show values well above 1 N, which is considered the lower limit for their proper use in a CLC unit [37]. In addition, there are four materials that present values above those obtained for the synthetic material prepared from raw metal oxides of chemical grade (2.7 N), namely MnSA, those prepared with MnGBHNE, and MnGBMPB with Fe-ore.

3.2. Analysis of the oxygen uncoupling capability

N_2/air cycles were performed to evaluate the oxygen uncoupling capability of the material, which happens when bixbyite is decomposed in N_2 to spinel. Table 3 shows the oxygen carrier capacity for cycles 1 and 3 due to the oxygen released in the oxygen uncoupling reaction, $R_{OC,CLOU}$. It is observed that most materials show a relatively large oxygen uncoupling capability for the first reduction in N_2. Remarkable are the high values observed for materials prepared with MnGBNHE as Mn source. On the contrary, the material prepared from MnSA showed a residual oxygen uncoupling capability. Nevertheless, the subsequent oxidation of spinel to bixbyite was very limited in all the cases, decreasing the oxygen uncoupling capability in successive redox cycles. Eventually, the oxygen transport capacity for oxygen uncoupling was significantly reduced to low values for cycle 3. Therefore, the relatively high values of conversion of spinel to bixbyite in the samples before the first cycle was deeply decreased in the third cycle. One example of the TGA curve for the CLOU tests can be found in Fig. S3 in SM. In any case, the regeneration of bixbyite from the spinel oxidation was extremely slow. Therefore, for practical purposes, relevant reactions with these oxygen carriers will not take into account the bixbyite phase, and from

Table 6
Rate index of the MnFe materials with different reacting gases.

Sample	Rate index (%/min)							
	H_2		CO		CH_4		O_2	
	Cycle 1	Cycle 3	Cycle 1	Cycle 3	Cycle 1	Cycle 3	Cycle 1	Cycle 3
MnSA	19.0	26.9	4.3	4.2	1.5	4.7	11.0	11.1
MnGBHNE+Fe-ESF	4.5	6.0	1.3	2.0	0.6	0.2	4.6	5.0
MnGBHNE+Fe-ore	6.7	7.7	1.0	0.6	1.7	0.8	8.6	6.7
MnGBMPB+Fe-ESF	20.6	20.1	4.7	3.7	6.3	3.3	12.1	10.5
MnGBMPB+Fe-ore	22.4	20.8	3.4	2.1	4.6	2.9	11.7	7.1
MnBR+Fe-ESF	23.3	18.9	4.7	3.0	4.8	3.3	12.4	11.2
MnBR+Fe-ore	23.9	24.3	4.8	3.0	4.9	2.8	11.8	12.3

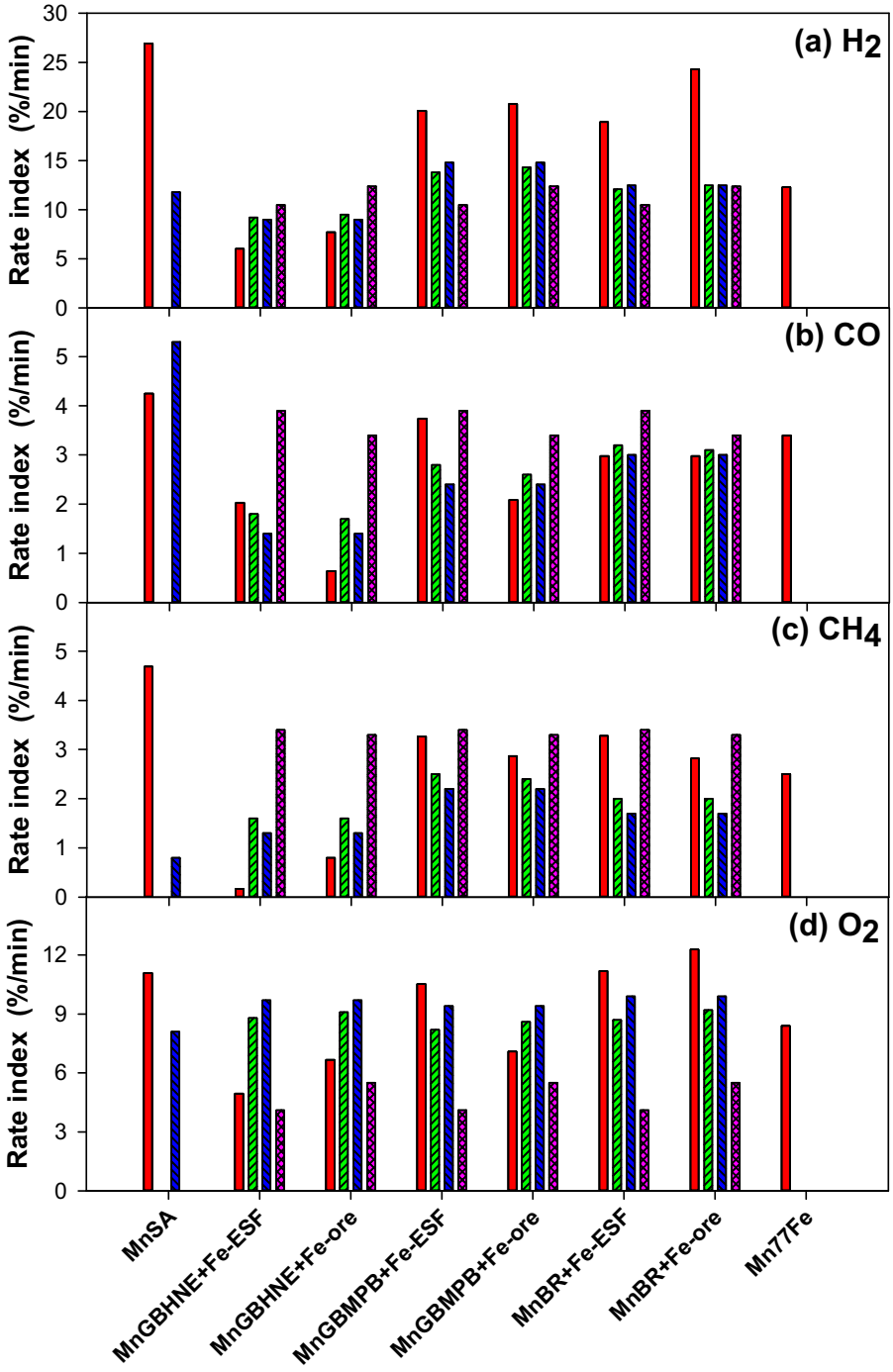

Fig. 3. Reactivity of the developed MnFe materials ( ) with H_2, CO, CH_4 and O_2 compared to those values for a physical mixture of the raw materials ( ), the raw Mn source ( ) and the raw Fe source ( ). Rate index for the synthetic Mn77Fe material produced from highly pure metal oxides is also included for comparison purposes. Data from [32,33,40].

now on we will analyze the reactivity of the materials considering the spinel as the most oxidized phase, similar to the Mn77Fe[SD]1350 material described in Table 2.

3.3. Reactivity of oxygen carriers with gaseous fuels

Reduction of the spinel phase happens in a reducing environment, e.g. when CH_4, CO or H_2 are present in the reacting gas. Reduction of spinel to mangano-wüstite is usual under CLC conditions [20]. However, further reduction to MnO + Fe may be of interest for the production of hydrogen by chemical looping with water splitting [38] or the use of CO_2 [39]. Therefore, both processes are here evaluated. The oxygen transport capacity depends on the reducing state. Thus, the oxygen transport capacity for the reduction of spinel to mangano-wüstite is $R_{OC} = 0.07$. Further reduction to MnO-Fe offers an additional oxygen transport capacity of $\Delta R_{OC} = 0.21 x_{Fe}$, which is a function of the Fe content in the oxygen carrier, x_{Fe}. Table 4 shows the theoretical values of the oxygen transport capacity for the active MnFe mixed oxide in the 7 prepared oxygen carriers, and the actual oxygen transport capacity considering the existing impurities in each material. One example of the

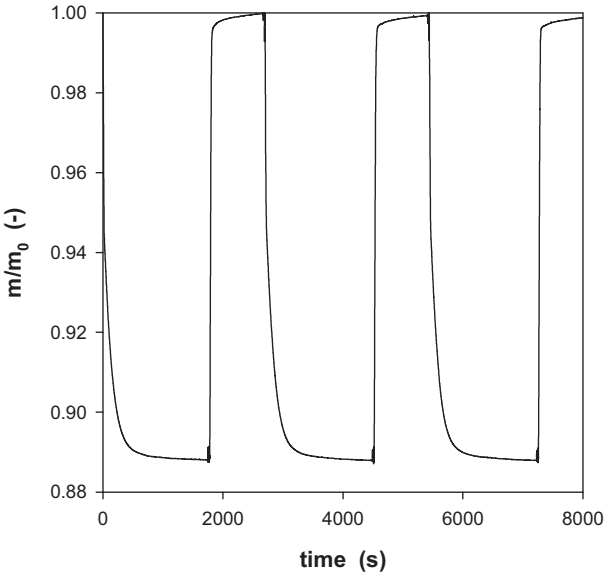

Fig. 4. Mass variation of the oxygen carrier sample based on MnSA ore during three redox cycles. Reduction: 15% H_2; Oxidation: air.

TGA curve for these CLC tests can be found in Fig. S4 in SM.

To evaluate the capability of the oxygen carrier to be reduced to mangano-wüstite, three redox cycles were performed in the TGA using 5% H_2 + 40% H_2O in the reduction period. These conditions would hinder further reduction of mangano-wüstite to a MnO + Fe mixture. Fig. 2 shows the solids conversion reached during the first and third reduction period. It can be seen that in the case of MnSA, the conversion achieved is 99%. Values between 87 and 90% were obtained for materials based on MnGBMPB and MnBR while for those containing MnGBHNE they were lower (70–75%). These results indicate that the reduction capacity of the formed spinel decreases according to the manganese source in the order MnSA > MnGBMPB ≈ MnBR > MnGBHNE. Smaller differences were found depending on the iron source, but somewhat higher values were found for Fe-ore compared to Fe-ESF. In addition, the conversion values barely changed in the three redox cycles, as well as the solids conversion reached during the oxidation period showed similar values. This result highlights the good recyclability and stability of the materials with the redox cycles.

Fig. 2 also gives the conversion for reduction in 15%CH_4 or 15% CO for cycles 1 and 3. There are hardly differences from cycle 1 to 3 with CO (variations less than 5%) except with the materials based on MnGBHNE: mixed with Fe-ESF the reduction degree decreased from 67% in cycle 1 to 48% in cycle 3; when mixed with Fe-ore this decrease was from 96 to 86%. It is noticed that the conversion of MnSA with CO reach values higher than 1, which indicates that some mangano-wüstite is further reduced to MnO + Fe. One possible explanation for this behavior is the deposition of solid carbon on the oxygen carrier surface, which may react with mangano-wüstite to form the MnO + Fe mixture.

However, a general reduction in the solids conversion was observed with CH_4 for all the materials, except for MnSA, which slightly increases (5%) from cycle 1 to 3, achieving the highest conversions with CH_4 (81%). It is well noting that lower conversions are obtained for CH_4 as compared with the rest of gases. It should be highlighted the low conversions achieved for the MnGBHNE+Fe-ESF material, but also the relatively high conversion shown by MnSA with CH_4, which in general is a gas with lower reactivity with oxygen carriers.

Table 5 shows the actual oxygen transport capacity during reduction with 5%H_2 + 40%H_2O compared to those values estimated for a physical mixture of the different Mn- and Fe-based raw materials considering the molar ratio Mn/Fe previously calculated from each sample; see Table 2. In a physical mixture, the oxygen transference in the Mn-based materials happens in the Mn_3O_4/MnO redox system, which is similar to the oxidation state of Mn considering the MnFe mixed oxide in the spinel/mangano-wüstite system. However, iron oxide phase moves from Fe_3O_4 to FeO in the MnFe mixed oxides, but it reacts from Fe_2O_3 to Fe_3O_4 in a mono-metallic material. Then, the oxygen transport capacity of iron in the MnFe mixed oxide (R_{OC} = 6.9%) is higher than that in the mono-metallic raw material (R_{OC} = 3.3%). Thus, higher values for the MnFe mixed oxide compared to a physical mixture of raw materials are found for oxygen carriers with a solids conversion ≥0.9 in Fig. 2. This difference is remarkably higher for the MnFe mixed oxide from MnSA because the MnFe mixed oxide is not formed during calcination of the raw MnSA ore [32]. However, this advantage is lost when the solids conversion of the MnFe mixed oxides are lower than 0.9.

In addition to the oxygen transport capacity, the reactivity of the oxygen carrier material is a key parameter to be evaluated. With this purpose, the rate index was calculated for the different fuel gases in the 7 mixed oxides, see Table 6. Interestingly, the rate index for the first cycle was different to those in subsequent cycles, and then stabilized. However, there was not a clear trend on the increase or decrease of the rate index with the redox cycles. Major changes were the increase in the reactivity shown by MnSA with H_2 and CH_4. But reactivity with CH_4 decreased for the other materials. Minor changes were observed for the oxidation reaction. In general, the rate index values followed the order $H_2 > O_2 > CO \approx CH_4$. But low reactivity with H_2 was shown by materials prepared from MnGBHNE. In general, MnSA presented the best performance.

The evaluation of the reactivity of the MnFe materials may be done by comparing the Rate index values with those values obtained for other oxygen carrier materials. Fig. 3 shows that the reactivity of most of MnFe oxygen carriers prepared with low-cost raw materials is higher (H_2, CH_4 and O_2) or similar (CO) than the reactivity of the twin material Mn77Fe prepared from highly pure metal oxides by Pérez-Vega et al. [33]. In general, the materials prepared from MnGBHNE have a lower reactivity than the raw materials or a physical mixture of them. Materials prepared from MnGBMPB and MnBR have similar reactivity to, at least, one of the raw material used as Mn or Fe source for CO, CH_4 and O_2. However, the reactivity for H_2 is higher for the materials forming the MnFe mixed oxide, which were prepared in this work. Finally, it is noteworthy the high reactivity showed by the oxygen carrier based on the MnSA material prepared in this study. This natural ore has itself a suitable Mn and Fe content to form the desired MnFe mixed oxide. However, it was confirmed that the pre-grinding step proposed in this work promoted the formation of the MnFe mixed oxide, which resulted in an increase in the reactivity with H_2, CH_4 and O_2 compared to the raw material.

It is known that mangano-wüstite may be further reduced to a MnO + Fe mixture, which may be of interest for the CLWS process. A deep reduction of iron oxide to metallic iron often origins the deactivation of the oxygen carrier material by agglomeration of particles or sintering of the porous structure, which eventually causes a high decrease in the oxygen transport capacity. A preliminary evaluation of the recyclability of the materials under this situation was done by the complete conversion to MnO + Fe reacting with 15% H_2. The theoretical oxygen transport capacity of the materials for the Spinel-(MnO + Fe) redox pair was shown in Table 4. The solids conversion reached during reduction in H_2 was found to be close to the unity in all the cases, which means that the reduction of spinel to MnO + Fe was completed in H_2. As an example, the evolution of the mass sample during the three cycles performed in TGA for the oxygen carrier based on the MnSA ore is shown in Fig. 4. It can be observed that the material could be fully regenerated during the oxidation step and it showed good stability with the redox cycles. Also, no evidences of sintering or agglomeration was observed after the examination of reacted particles. Nevertheless, more studies would be required to evaluate the suitability of this material when a deep reduction to MnO + Fe was cyclically repeated during hundreds of redox cycles.

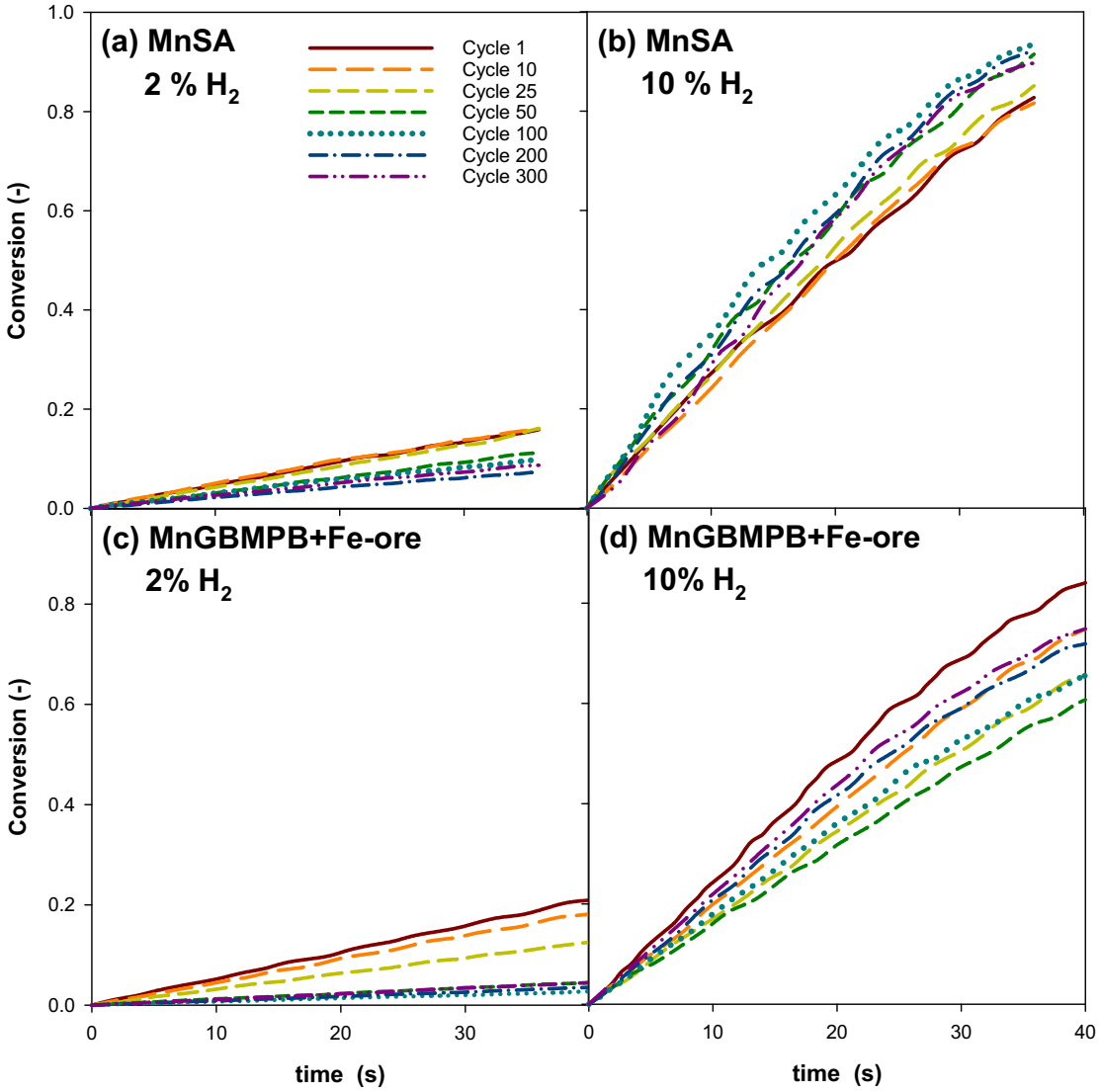

Fig. 5. Oxygen carrier conversion as a function of time at 950°C under 300 redox cycles for MnSA (a, b) and MnGBMPB+Fe-ore (c, d). Reduction conditions: (a) 2% H_2, 36 s; (b) 10% H_2, 36 s; (c) 2% H_2, 42 s; (d) 10% H_2, 42 s. Oxidation conditions: 10% O_2, 120 s allowing complete spinel regeneration.

Considering all parameters evaluated in this work, such as crushing strength, magnetism, oxygen transport capacity, reactivity to reducing gases and stability with redox cycles, MnSA and MnGBMPB+Fe-ore may be suitable materials to be used as oxygen carriers in CLC. MnSA was selected due to its high *Rate Index* values compared to others, especially with H_2 and CH_4. In addition, the crushing strength is also high (3.0 N). Materials prepared from MnGBMPB or MnBR showed similar performance. Even though both materials prepared by using the Tierga Fe-ore as the iron source have higher R_{OC} values than the estimated from the physical mixture of the raw materials (approx. 10% of enhancement) and good rate index for CH_4 (2.87 and 2.82%/min, respectively), the mixed oxide material prepared with MnGBMPB has higher mechanical strength (3.1 N vs. 2.5 N) and magnetic permeability (1.7 vs. 1.5). Materials based on MnGBHNE ore as Mn source were discarded as it obtains the lowest reaction conversions and *Rate Index* for all gases. Therefore, MnSA and MnGBMPB+Fe-ore materials are selected for further evaluation.

3.4. Analysis of long redox cycles for MnSA and MnGBMPB+Fe-ore mixed oxides

Considering all the above mentioned, MnSA and MnGBMPB+Fe-ore were selected for a long-term operation in the TGA by performing 300 redox cycles. Previous tests were performed by forcing the particles to completely react during the oxidation and reduction stages, which means high variation in the solids conversion. However, the variation in the solids conversion in a CLC unit depends on the solids circulation rate. Thus, a high variation in the solids conversion corresponds to a solids circulation rate slightly above the stoichiometric value to transport the required oxygen for the fuel combustion. Then, the variation of the solids conversion in a CLC unit decreases as the solids circulation rates increases. To evaluate the effect of different variation of solids conversion, the reduction and oxidation conditions were designed to achieve low (approx. 20%) and high (approx. 80%) conversions of the materials in the reduction of spinel to mangano-wüstite, in a similar way that was previously described by Cabello et al. [9]. For practical purposes, Fig. 5 depicts the conversion curves of the two oxygen carriers after several reduction cycles: 1,10, 25, 50, 100, 200 and 300.

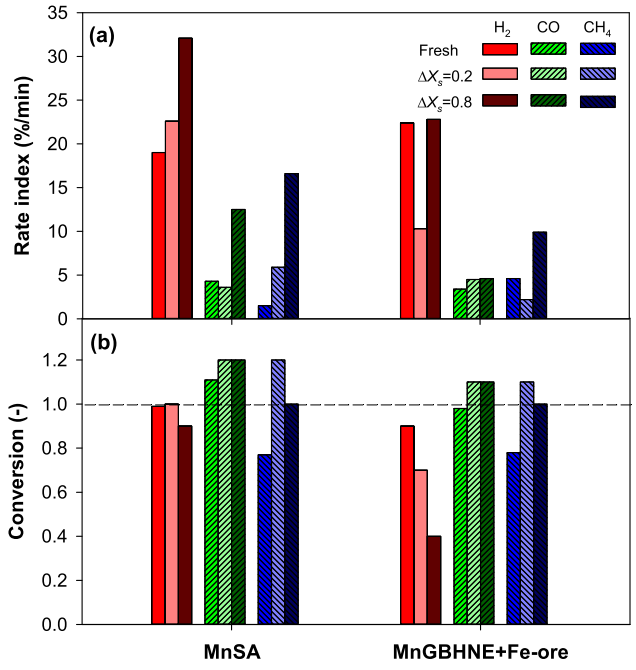

Fig. 6. (a) Reactivity and (b) solids conversion for fresh MnSA and MnGBMPB+Fe-ore oxygen carriers with H_2, CO and CH_4, and those of reacted particles after 300 redox cycles with low (ΔX_s = 20%) and high (ΔX_s = 80%) variation of the solids conversion.

Concerning MnSA, subjecting the material to low conversions (approx. 20%), the reaction rate with 2% H_2 notoriously decreased from cycle 25. To evaluate changes in reactivity, standard conditions should be used. Thus, the *Rate Index* values for H_2, CO, CH_4, and O_2 of cycled particles were also determined. Variation in the oxidation reactivity was of low relevance. Interestingly, reactivity with H_2 and CO barely changed; but reactivity with CH_4 was appreciably improved; see Fig. 6 (a). In addition, the mechanical resistance of the particles was negatively affected as the crushing strength decreased from 3.0 to 0.6 N.

A different behavior was observed when the ΔX_s was increased to ca. 80%. In this case, the solids conversion increased with the number of redox cycles. Regarding *Rate Index* values, they also increased with all reducing gases; see Fig. 6(a). Note that the *Rate Index* obtained with CO was nearly 4-fold higher while for CH_4 the reactivity rises as a factor of 10. Although the chemical stability of the MnFe mixed oxide was confirmed by XRD analysis (see Fig. S2(a) in SM), the volume of the particles greatly increased and part of the sample overflowed from the basket in the TGA; see Fig. S5 in SM. When the material was recovered from the basket, it was easily converted to fine dust; thus, the particle integrity was severely damaged by the redox cycles under high ΔX_s values.

Interestingly, the behavior of the MnGBMPB+Fe-ore oxygen carrier was quite different to that of MnSA. When the MnGBMPB+Fe-ore oxygen carrier reacted at low variation of the solids conversion (approx. 20%), it suffered a deep deactivation during the first 100 cycles when reacted with 2% H_2; see Fig. 5. Then, it was slightly re-activated, but eventually it showed only a small fraction of initial reactivity after 300 cycles. In this case, the *Rate Index* with H_2 and CH_4 was negatively affected, although for CO slightly increased. The crushing strength value hardly changed from the original material: 2.9 N vs. 3.1 N.

When reaction progressed under relatively high variation of solids conversion values ($\Delta X_s \approx$ 80%), it slowly deactivates to a minimum reactivity by 50 cycles; but then, it re-activated later significantly by 300 cycles, approaching to the reactivity shown by the fresh material; see Fig. 5. Thus, the eventual *Rate Index* values for H_2 and CO barely changed; but it was highly increased with CH_4; see Fig. 6(a). The chemical stability of the MnFe mixed oxide was confirmed (see Fig. 2(b) in SM). Crushing strength reduced to 1.6 N, which is still higher than the threshold value of 1.0 N.

In addition, the variation in the reducing capability of cycled materials was evaluated under the standard condition previously used for fresh materials in Fig. 2, and the solids conversion was determined after reduction at 5% H_2 + 40% H_2O, 15% CO + 20% CO_2 or 15% CH_4 + 20% H_2O; see Fig. 6(b). In general, the conversion was improved in cycled particles, especially with CH_4 in both tested cases, namely low and high ΔX_s values. But for H_2 the R_{OC} values are practically maintained for MnSA while for MnGBMPB+Fe-ore they are significantly reduced by 30% when the material was subjected to low conversions, and by 60% at high conversions.

Morphologic changes in the oxygen carrier particles after 300 cycles were observed by SEM-EDX. Fig. 7 shows the SEM pictures for fresh MnSA material (a–b) and after submitted to 300 redox cycles applying low – ca. 20% – (c–d) and high – ca. 80% – (e–f) variation in the solids conversion. Images in Fig. 7 (b), (d) and (f) were taken from particles embedded in a resin and dry fractured for a cross-section visualization.

Some changes were observed when the variation of the solids conversion was low. Mainly, some sinterization was observed with the formation of pores bigger than those existing in the fresh particles. However, the EDX line-scan profile does not suggest any relevant preferential migration of Mn or Fe in the particle. A closer examination of the external surface of the particles in Fig. 8 shows the appearance of a coating with zones or points with an increase in the composition of Mn. This finding suggests the existence of a transition of a solid state migration of Mn from the inner side of the particle to the outer side creating a thin layer in the surrounding of the particle containing preferentially Mn.

The MnSA-based particles suffered a significant change in their morphology when high conversions are used (ca. 80%). The particles lose their initial appearance, linked with the greater porosity in the interior of the particle while structural changes due to the chemical stress on the particles occurred. The increase in porosity was previously intuited from the picture of Fig. S5 in SM. In addition, the integrity of the particles is severely affected, appearing small particles detached from main particles and a feeble structure in individual particles. In Fig. 7(e) it can be also observed some small particles surrounding the MnSA material corresponding to Mn for the corresponding line-scan; see Fig. 7 (f). This fact suggests the migration and sinterization of Mn particles from the inner side of the particles to the outer side was promoted by the increase in the variation of the solids conversion in the redox cycles.

Fig. 9 shows the SEM micrographs of cross-section for the MnGBMPB+Fe-ore oxygen carrier particles, for fresh particles and cycled both for low (ca. 20%) and high (ca. 80%) variation of solids conversion. In this case, particles maintained their integrity and the inner morphology of the materials was practically preserved, with only a slight increase of the porosity by applying the redox cycles. Nevertheless, some small particles detached from the main particles and containing mainly Mn are observed when the variation of solids conversion was 80%, related to the effect of chemical stress on the mechanical strength of the particles, as previously discussed.

4. Conclusions

Oxygen carrier particles based on MnFe mixed oxides were prepared by using low-cost Mn and Fe raw materials as Mn and Fe sources, namely four Mn-ore, one Fe-ore and one Fe-based industrial waste. Pre-grinding to reduce the particle size of the minerals before the preparation of the oxygen carrier particles had a positive effect on the achievement of the MnFe mixed oxide; otherwise it was not obtained. In all cases, the MnFe mixed oxide was oxidized to spinel phase, which provides the particles with magnetic properties. Then, reduction to mangano-wüstite was observed in the presence of a reducing gas, such as H_2, CO or CH_4.

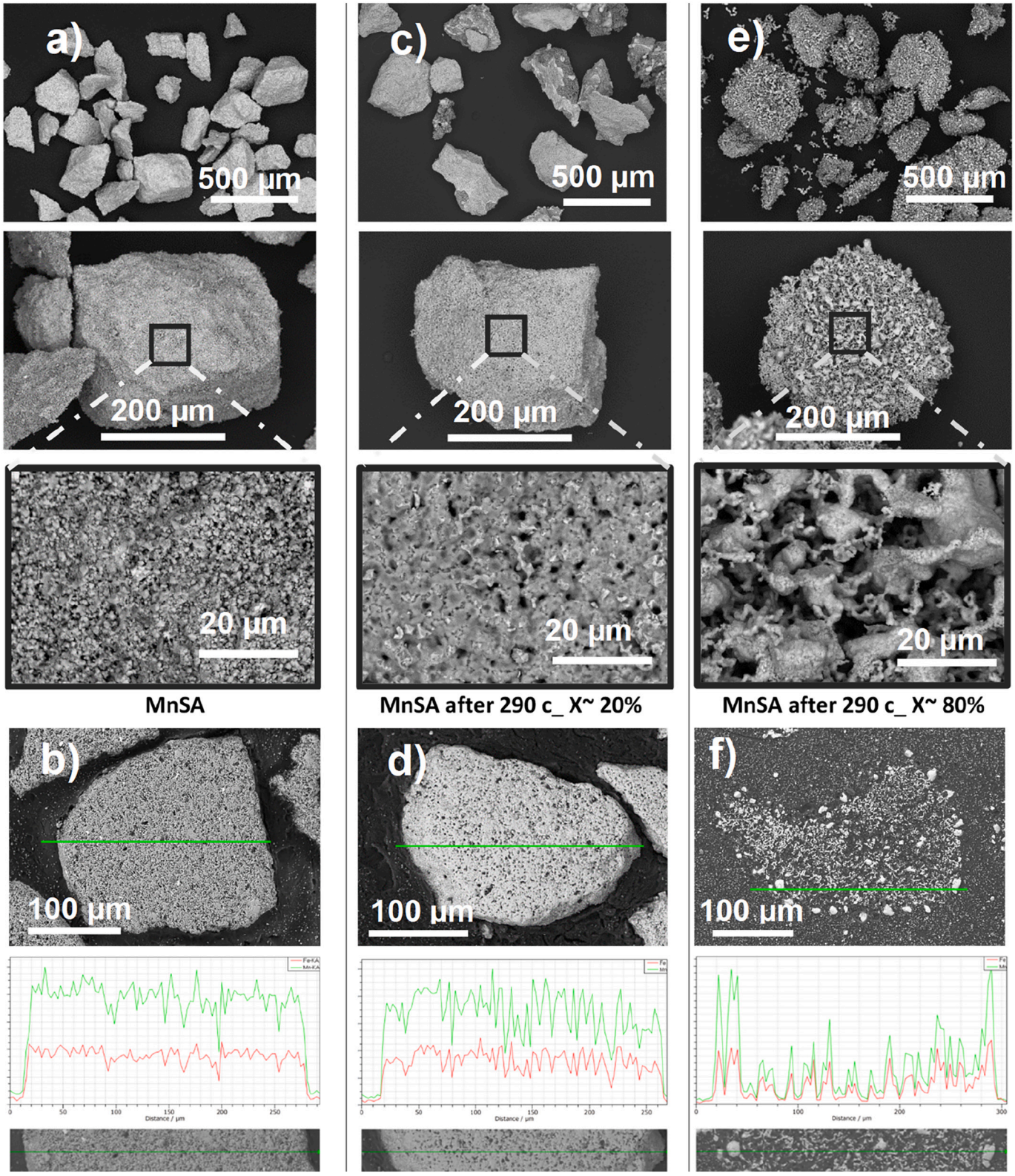

Fig. 7. SEM images of (a–b) fresh MnSA; and after 300 redox cycles at 950°C: (c–d) variation of solids conversion of ca. 20%; (e–f) variation of solids conversion of ca. 80%. (b), (c), and (f) show the EDX line-scan for Mn and Fe elements in a cross-section of the particles (cut particles).

Oxidation of spinel to bixbyite did not happen in a relevant extension, and therefore the oxygen uncoupling capability of MnFe mixed oxides could not be exploited for the prepared materials.

Oxygen carrier based on the use of South African Mn-ore (MnSA) as Mn and Fe source, as well as a mixture of Mn-ore from Gabon (MnGBMPB) and Tierga Fe-ore were selected due to their good performance accounting for reactivity, oxygen transport capacity and crushing strength of the particles. Reactivity was even higher than that showed by a similar material prepared from highly pure metal oxides. A long-term evaluation of these materials revealed that the oxygen carrier based on

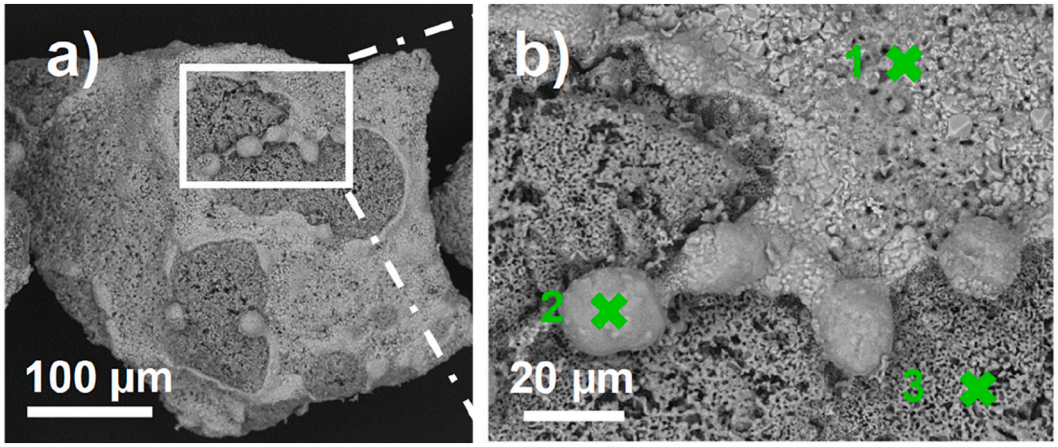

Sp Nº	Mn (wt%)	Fe (wt%)
1	33.2	14.1
2	56.3	4.3
3	14.4	14.9

Fig. 8. (a) SEM images of MnSA after 300 redox cycles at 950°C with conversion of ca. 20%, (b) inset of (a) including 3 spectrum section analyzed by EXD, (c) elemental compositions for Mn and Fe (wt%).

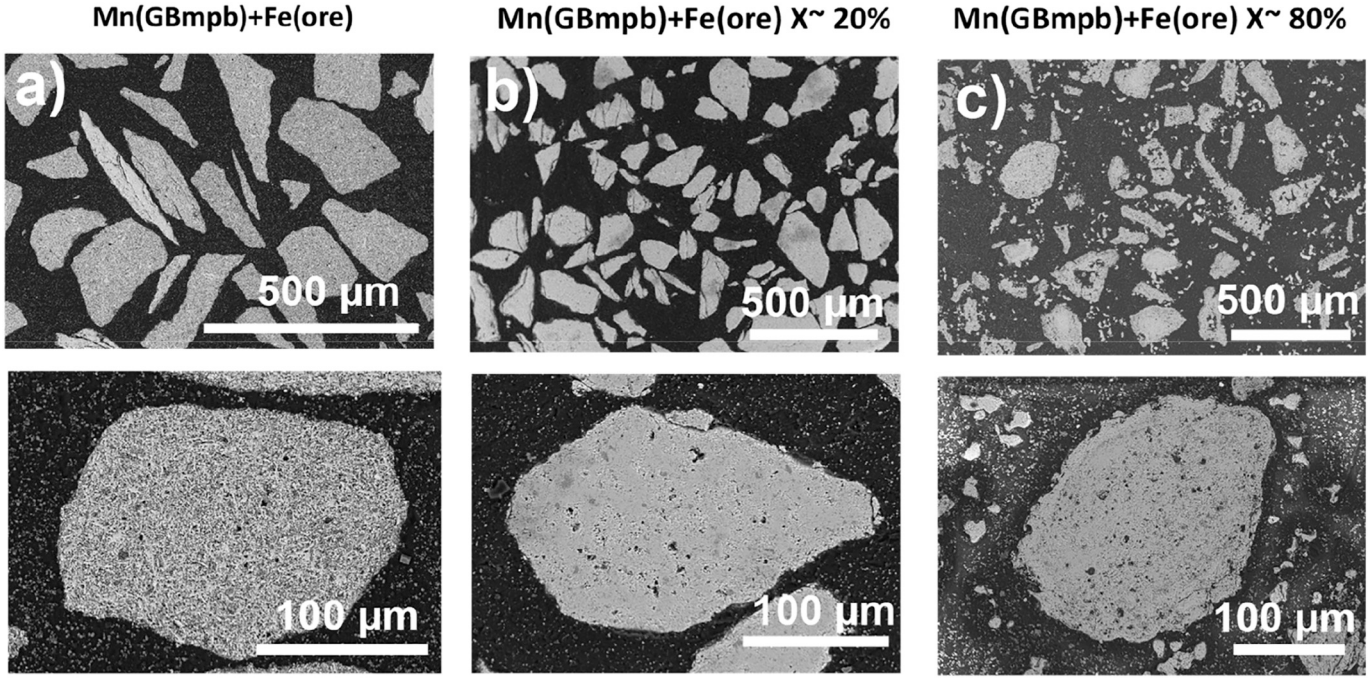

Fig. 9. SEM micrographs of MnGBMPB+Fe-ore oxygen carrier for (a) fresh particles; and cycled particles at 950°C with (b) variation of solids conversion of ca. 20%, and (c) variation of solids conversion of ca. 80%.

MnSA increased its reactivity but suffered from strong chemical stress, with a decrease in the crushing strength of particles. Catastrophic effect on the particles was observed when the variation of the solids conversion was high (ca. 80%). Particles based on MnGBMPB+Fe-ore maintained their mechanical integrity to acceptable values, but some deactivation was observed when the variation of the solids conversion was low (ca. 20%) during the redox cycles. Therefore, the use of the MnGBMPB+Fe-ore material is recommended under conditions allowing a relatively high variation of the solids conversion (ca. 80%). Under these conditions, reactivity with H_2 and CO was similar to the original particles, or even increased for CH_4.

CRediT authorship contribution statement

Beatriz Zornoza: Conceptualization, Methodology, Validation, Formal analysis, Investigation, Data curation, Writing – original draft, Visualization. **Teresa Mendiara:** Conceptualization, Methodology, Validation, Investigation, Writing – review & editing, Supervision. **Alberto Abad:** Conceptualization, Methodology, Validation, Investigation, Resources, Writing – review & editing, Supervision, Project administration, Funding acquisition.

Declaration of Competing Interest

The authors declare that they have no known competing financial interests or personal relationships that could have appeared to influence the work reported in this paper.

Acknowledgments

This work was supported by the SWINELOOP project (PID2019-106441RB-I00/AEI/10.13039/501100011033). B.Z. acknowledges the "Juan de la Cierva" Program (IJCI-2016-30776). Authors thanks PROMINDSA for supplying Tierga Fe-ore; Alcoa Europe-Alúmina

Española S.A. for providing redmud (Fe-ESF); Ferroatlántica del Cinca S. L. (former Hidro Nitro Española S.A.) for providing MnSA and MnGBHNE materials; Mario Pilato Blatt S.A. for providing MnGBMPB; and Leopoldo Alcázar (CT-GAS) for providing the MnBR material.

Appendix A. Supplementary data

Supplementary data to this article can be found online at https://doi.org/10.1016/j.fuproc.2022.107313.

References

[1] L. Zeng, Z. Cheng, J.A. Fan, L.-S. Fan, J. Gong, Metal oxide redox chemistry for chemical looping processes, Nat. Rev. Chem. 2 (2018) 349–364, https://doi.org/10.1038/s41570-018-0046-2.
[2] T. Mattisson, M. Keller, C. Linderholm, P. Moldenhauer, M. Rydén, H. Leion, A. Lyngfetl, Chemical-looping technologies using circulating fluidized bed systems: status of development, Fuel Process. Technol. 172 (2018) 1–12, https://doi.org/10.1016/j.fuproc.2017.11.016.
[3] T. Song, L. Shen, Review of reactor for chemical looping combustion of solid fuels, Int. J. Greenh. Gas Control 76 (2018) 92–110, https://doi.org/10.1016/j.ijggc.2018.06.004.
[4] T. Gauthier, M. Yazdanpanah, A. Forret, B. Amblard, A. Lambert, S. Bertholin, CLC, a promising concept with challenging development issues, Powder Technol. 316 (2017) 3–17, https://doi.org/10.1016/j.powtec.2017.01.003.
[5] J. Adánez, A. Abad, Chemical-looping combustion: status and research needs, Proc. Combust. Inst. 37 (2019) 4303–4317, https://doi.org/10.1016/j.proci.2018.09.002.
[6] S.C. Bayham, A. Tong, M. Kathe, L.-S. Fan, Chemical looping technology for energy and chemical production, WIREs Energy Environ. 5 (2016) 216–241, https://doi.org/10.1002/wene.173.
[7] M. Rajabi, M. Mehrpooya, Z. Haibo, Z. Huang, Chemical looping technology in CHP (combined heat and power) and CCHP (combined cooling heating and power) systems: a critical review, Appl. Energy 253 (2019) 113544, https://doi.org/10.1016/j.apenergy.2019.113544.
[8] A. Abad, Chemical looping for hydrogen production, in: Paul Fennell, Ben Anthony (Eds.), Calcium and Chemical Looping Technology for Power Generation and CO_2 Capture, Woodhead Publishing/Elsevier, 2015.
[9] A. Cabello, A. Abad, M.T. Izquierdo, P. Gayán, L.F. de Diego, F. García-Labiano, J. Adánez, Qualification of operating conditions to extend oxygen carrier utilization in the scaling up of chemical looping processes, Chem. Eng. J. 430 (2022) 132602, https://doi.org/10.1016/j.cej.2021.132602.
[10] A. Cabello, T. Mendiara, A. Abad, M.T. Izquierdo, F. García-Labiano, Production of hydrogen by chemical looping reforming of methane and biogas using a reactive and durable Cu-based oxygen carrier, Fuel 322 (2022) 124250, https://doi.org/10.1016/j.fuel.2022.124250.
[11] T. Mattisson, A. Lyngfelt, H. Leion, Chemical-looping with oxygen uncoupling for combustion of solid fuels, Int. J. Greenh. Gas Control 3 (2009) 11–19, https://doi.org/10.1016/j.ijggc.2008.06.002.
[12] J. Adánez, A. Abad, T. Mendiara, P. Gayán, L.F. de Diego, F. García-Labiano, Chemical looping combustion of solid fuels, Prog. Energy Combust. Sci. 65 (2018) 6–66, https://doi.org/10.1016/j.pecs.2017.07.005.
[13] A. Lyngfelt, Chemical looping combustion: status and development challenges, Energy Fuel 34 (2020) 9077–9093, https://doi.org/10.1021/acs.energyfuels.0c01454.
[14] T. Mendiara, P. Gayán, A. Abad, F. García-Labiano, L.F. de Diego, J. Adánez, Characterization for disposal of Fe-based oxygen carriers from a CLC unit burning coal, Fuel Process. Technol. 138 (2015) 750–757, https://doi.org/10.1016/j.fuproc.2015.07.019.
[15] V. Andersson, A.H. Soleimanisalim, X. Kong, H. Leion, T. Mattisson, J.B. C. Pettersson, Alkaly interactions with a calcium manganite oxygen carrier used in chemical looping combustion, Fuel Process. Technol. 227 (2022) 107099, https://doi.org/10.1016/j.fuproc.2021.107099.
[16] D. Mei, A.H. Soleimanisalim, C. Linderholm, A. Lyngfelt, T. Mattisson, Reactivity and lifetime assessment of an oxygen releasable manganese ore with biomass fuels in a 10 kW_{th} pilot rig for chemical looping combustion, Fuel Process. Technol. 215 (2021) 106743, https://doi.org/10.1016/j.fuproc.2021.106743.
[17] M. Rydén, H. Leion, T. Mattisson, A. Lyngfelt, Combined oxides as oxygen-carrier material for chemical-looping with oxygen uncoupling, Appl. Energy 113 (2014) 1924–1932, https://doi.org/10.1016/j.apenergy.2013.06.016.
[18] A. Shulman, E. Cleverstam, T. Mattisson, A. Lyngfelt, Manganese/iron, manganese/nickel, and manganese/silicon oxides used in chemical-looping with oxygen uncoupling (CLOU) for combustion of methane, Energy Fuel 23 (2009) 5269–5275, https://doi.org/10.1021/ef9005466.
[19] M. Abián, A. Abad, M.T. Izquierdo, P. Gayán, L.F. de Diego, F. García-Labiano, J. Adánez, Titanium substituted manganese-ferrite as an oxygen carrier with permanent magnetic properties for chemical looping combustion of solid fuels, Fuel 195 (2017) 38–48, https://doi.org/10.1016/j.fuel.2017.01.030.
[20] A. Abad, R. Pérez-Vega, L.F. de Diego, P. Gayán, M.T. Izquierdo, F. García-Labiano, J. Adánez, Thermochemical assessment of chemical looping assisted by oxygen uncoupling with a MnFe-based oxygen carrier, Appl. Energy 251 (2019) 113340, https://doi.org/10.1016/j.apenergy.2019.113340.
[21] R. Pérez-Vega, A. Abad, F. García-Labiano, P. Gayán, L.F. de Diego, M.T. Izquierdo, J. Adánez, Chemical looping combustion of gaseous and solid fuels with manganese-iron mixed oxide as oxygen carrier, Energy Convers. Manag. 159 (2018) 221–231, https://doi.org/10.1016/j.enconman.2018.01.007.
[22] G. Azimi, H. Leion, M. Rydén, T. Mattisson, A. Lyngfelt, Investigation of different Mn−Fe oxides as oxygen carrier for chemical-looping with oxygen uncoupling (CLOU), Energy Fuel 27 (2013) 367–377, https://doi.org/10.1021/ef301120r.
[23] G. Azimi, M. Rydén, H. Leion, T. Mattisson, A. Lyngfelt, $(Mn_zFe_{1-z})_yO_x$ combined oxides as oxygen carrier for chemical-looping with oxygen uncoupling, AICHE J. 59 (2013) 582–588, https://doi.org/10.1002/aic.13847.
[24] S. Bhavsar, B. Tackett, G. Veser, Evaluation of iron- and manganese-based mono- and mixed-metallic oxygen carriers for chemical looping combustion, Fuel 136 (2014) 268–279, https://doi.org/10.1016/j.fuel.2014.07.068.
[25] P. Hallberg, M. Hanning, M. Rydén, T. Mattisson, A. Lyngfelt, Investigation of a calcium manganite as oxygen carrier during 99 h of operation of chemical-looping combustion in a 10 kW_{th} reactor unit, Int. J. Greenh. Gas Control 53 (2016) 222–229, https://doi.org/10.1016/j.ijggc.2016.08.006.
[26] M. Jacobs, T. van der Kolk, K. Albertsen, T. Mattisson, A. Lyngfelt, F. Snijkers, Synthesis and upscaling of perovskite Mn-based oxygen carrier by industrial spray drying route, Int. J. Greenh. Gas Control 70 (2018) 68–75, https://doi.org/10.1016/j.ijggc.2018.01.006.
[27] R. Siriwardane, H. Tian, T. Simonyi, J. Poston, Synergetic effects of mixed copper-iron oxides oxygen carriers in chemical looping combustion, Fuel 108 (2013) 319–333, https://doi.org/10.1016/j.fuel.2013.01.023.
[28] X. Tian, H. Zhao, J. Ma, Cement bonded fine hematite and copper ore particles as oxygen carrier in chemical looping combustion, Appl. Energy 204 (2017) 242–253, https://doi.org/10.1016/j.apenergy.2017.07.025.
[29] Y. Dong, Y. Wang, J. Ma, H. Bu, C. Zheng, H. Zhao, Binary-ore oxygen carriers prepared by extrusion–spheronization method for chemical looping combustion of coal, Fuel Process. Technol. 221 (2021) 106921, https://doi.org/10.1016/j.fuproc.2021.106921.
[30] Z. Su, Y. Wang, H. Du, J. Ma, Y. Zheng, H. Zhao, Using copper ore and hematite fine particles as raw materials of an oxygen carrier for chemical looping combustion of coal: spray drying granulation and performance evaluation, Energy Fuel 34 (2020) 8587–8599, https://doi.org/10.1021/acs.energyfuels.0c01023.
[31] Y. Wang, X. Tian, H. Zhao, K. Liu, H. Bu, Y. Dong, Z. Su, C. Zheng, Synergetic effects of cement bonded copper ore and red mud as oxygen carrier during in-situ gasification chemical looping combustion of coal char, Fuel 303 (2021) 121295, https://doi.org/10.1016/j.fuel.2021.121295.
[32] D. Mei, T. Mendiara, A. Abad, L.F. de Diego, F. García-Labiano, P. Gayán, J. Adánez, H. Zhao, Evaluation of manganese minerals for chemical looping combustion, Energy Fuel 29 (2015) 6605–6615, https://doi.org/10.1021/acs.energyfuels.5b01293.
[33] R. Pérez-Vega, A. Abad, P. Gayán, L.F. de Diego, F. García-Labiano, J. Adánez, Development of $(Mn_{0.77}Fe_{0.23})_2O_3$ particles as an oxygen carrier for coal combustion with CO_2 capture via in-situ gasification chemical looping combustion (iG-CLC) aided by oxygen uncoupling (CLOU), Fuel Process. Technol. 164 (2017) 69–79, https://doi.org/10.1016/j.fuproc.2017.04.019.
[34] T. Mendiara, L.F. de Diego, F. García-Labiano, P. Gayán, A. Abad, J. Adánez, On the use of a highly reactive iron ore in chemical looping combustion of different coals, Fuel 126 (2014) 239–249, https://doi.org/10.1016/j.fuel.2014.02.061.
[35] T. Mendiara, L.F. de Diego, F. García-Labiano, P. Gayán, A. Abad, J. Adánez, Behaviour of a bauxite waste material as oxygen carrier in a 500 Wth CLC unit with coal, Int. J. Greenh. Gas Control 17 (2013) 170–182, https://doi.org/10.1016/j.ijggc.2013.04.020.
[36] M. Johansson, T. Mattisson, A. Lyngfelt, Investigation of Mn_3O_4 with stabilized ZrO_2 for chemical-looping combustion, Chem. Eng. Res. Design 84 (A9) (2006) 807–818, https://doi.org/10.1205/cherd.05206.
[37] M. Johansson, T. Mattisson, A. Lyngfelt, Investigation of Fe_2O_3 with $MgAl_2O_4$ for chemical-looping combustion, Ind. Eng. Chem. Res. 43 (2004) 6978–6987, https://doi.org/10.1021/ie049813c.
[38] G. Voitic, V. Hacker, Recent advancements in chemical looping water splitting for the production of hydrogen, RSC Adv. 6 (2016) 98267, https://doi.org/10.1039/c6ra21180a.
[39] J. Hu, V.V. Galvita, H. Poelman, G.B. Marin, Advanced chemical looping materials for CO_2 utilization: a review, Materials 11 (2018) 1187, https://doi.org/10.3390/ma11071187.
[40] T. Mendiara, R. Pérez, A. Abad, L.F. de Diego, F. García-Labiano, P. Gayán, J. Adánez, Low-cost Fe-based oxygen carrier materials for the iG-CLC Process with coal. 1, Ind. Eng. Chem. Res. 51 (2012) 16216–16229, https://doi.org/10.1021/ie302157y.